Nature and Science

Websites:
http://www.sciencepub.net/nature
http://www.sciencepub.net

Emails:
naturesciencej@gmail.com
editor@sciencepub.net

MARSLAND PRESS
Multidisciplinary Academic Journal Publisher

Synthesis, Characterization and Computational Studies on the Corrosion Inhibitive Potentials of (E)-3-(2-P-Tolyldiazenyl)-1-Nitrosonaphthalen-2-ol

J. S. Amoko[1,3], O. F. Akinyele[2**], O. E. Oyeneyin[1], D. S. Olayanju[2] and C. O. Aboluwoye[1]

[1.] Department of Chemical Sciences, Adekunle Ajasin University, Akungba-Akoko, Ondo State, Nigeria
[2.] Department of Chemistry, Obafemi Awolowo University, Ile-Ife, Nigeria
[3.] Department of Chemistry, Adeyemi College of Education, Ondo, Ondo State, Nigeria
ofakinyele@oauife.edu.ng

Abstract: A novel (E)-3-(2-P-Tolyldiazenyl)-1-nitrosonaphthalen-2-ol (NAD) was synthesized and characterized via Fourier Transform Infrared (FTIR), UV/Vis, ^{1}H-NMR and ^{13}C-NMR spectroscopic techniques. Weight loss analysis showed that this molecule possesses excellent corrosion inhibitive potentials. Variations of inhibition efficiency with concentration and temperature were observed and the results obtained showed that inhibition efficiency increases with increase in concentration while it reduces with an increase in temperature. The efficiency of this molecule was validated with theoretical models using the density functional theory (DFT) method with the hybrid functional, Becke Three Lee Yang Parr (B3LYP) correlation with 6-31G* basis set. It was observed that the molecule has very good corrosion inhibitive potentials.

[J. S. Amoko, O. F. Akinyele, O. E. Oyeneyin, D. S. Olayanju and C. O. Aboluwoye. **Synthesis, Characterization and Computational Studies on the Corrosion Inhibitive Potentials of (E)-3-(2-P-Tolyldiazenyl)-1-Nitrosonaphthalen-2-ol.** *Nat Sci* 2020;18(11):74-84]. ISSN 1545-0740 (print); ISSN 2375-7167 (online). http://www.sciencepub.net/nature. 7. doi:10.7537/marsnsj181120.07.

Keywords: DFT, Polarization, Activation parameters, Gravimetry, Azo-dye

1. Introduction

One of the most practical ways to prevent corrosion of metals and alloys in acidic media, a scourge peculiar to the oil and gas industries, is to use corrosion inhibitors, which are mainly organic compounds containing heteroatoms like sulphur, nitrogen, oxygen and phosphorus with lone pair of electrons and as a result facilitate adsorption on metal surfaces (Abiola and Otaigbe, 2009; Abiola and Otaigbe, 2008; Obot and Obi-Egbedi, 2011; Arukalam *et al.,* 2014). These inhibitors are added with the aim of reducing metal loss when in contact with acid media. Azo dyes possess π-electrons systems and heteroatoms in the moieties, this enhances adsorption on mild steel through the formation of covalent bonds (Solmaz, 2014; Ameh *et al.,* 2015). They are adsorbed on the metal surface by forming protective layers that prevent attacks by acid media used in pickling, descaling and oil well acidizing. Methods such as the gravimetric; which gives information about the average rate of corrosion and inhibition efficiency (Ameh *et al.,* 2015; Oguzie *et al.,* 2010; Naguib *et al.,* 2013 8), potentiodynamic polarization (Naguib *et al.,* 2013; Manbrouk *et al.,* 2017), electrochemical impedance spectroscopy (Fouda *et al.,* 2014), fourier transform infra-red (FTIR) spectroscopy (Ameh *et al.,* 2015) and scanning electron microscope (SEM) (Ameh *et al.,* 2015; Naguib et al., 2013) have been used for corrosion inhibition studies. Recently, quantum chemical calculations have been employed in investigating and predicting the corrosion inhibition potentials of molecules (Arukalam *et al.,* 2014; Ameh *et al.,* 2015; Oyeneyin, 2017; Kara *et al.,* 2012). This is because they can be used to explain physical parameters like reactivities and electronic behaviours. Since it is important to describe the electronic behaviours, the density functional theory (DFT) is usually used in predicting and understanding chemical processes like corrosion inhibition processes either as a method to validate experimental findings or solely to explain inhibitive potentials of organic molecules. Azo dyes have been extensively investigated and reported as corrosion inhibitors (Naguib *et al.,* 2013; Mabrouk *et al.,* 2017; Fouda *et al.,* 2014). This may be due to the ability of complex formation between metal-ions and the azo nitrogen binding at the electrode surface (Naguib *et al.,* 2013), steric effects and electron density of donor atoms (Elmsellem *et al.,* 2014). This work will therefore validate the findings from weight loss and potentiodynamic polarization experiments.

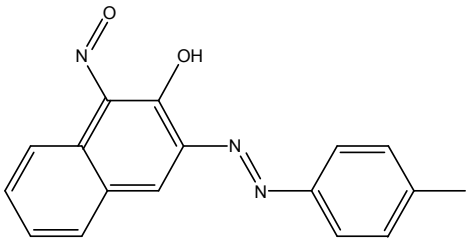

Figure 1: Synthesized azo dye (NAD)

2. Experimental

2.1 Preparation of Mild Steel

Commercially available mild steel was bought and mechanically machined into dimension 3 cm x 3 cm x 0.05 cm with hole at the centre for easy hooking. Each were polished with evenly gritted emery paper; washed with distilled water and degreased with acetone by dipping them in acetone for five minutes and dried over $CaCl_2$ in desiccators overnight (Geethamani and Kasthuri, 2015).

2.2 Synthesis of NAD

NAD was synthesized using the method reported in literature (Scheme 1.0) (Botros, 1977; Ahmadi and Amani, 2012). A suspension of *P*-Toluidine (2.8 g, 40 mmol) in hydrochloric acid (36 ml) and water (16 ml) was heated to around 70°C until complete dissolution. The clear solution poured into ice was diazotized below 5°C with sodium nitrite (2.8 g, 40 mmol) dissolved in water (10 ml). The resulting cold diazonium solution was then added slowly with continuous vigorous stirring over the course of 45 mins at 0°C to a solution of 1-nitrosol-2-naphatol (6.92 g, 40 mmol) in water (75 ml) containing sodium hydroxide (1.6 g) and sodium carbonate (14.8 g). The product was collected by filtration and washed with water then later recrystallized from ethanol three times.

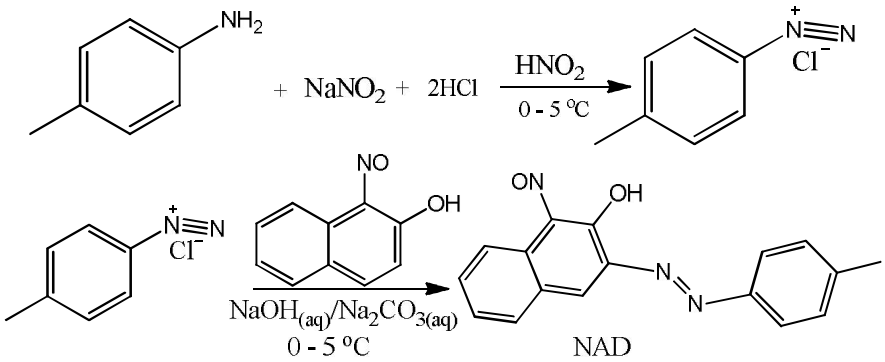

Scheme 1.0: Synthetic route of NAD

The synthesized brownish-yellow molecule has a chemical formula of $C_{17}H_{16}N_3O_2$, molecular weight of 294.334, melting point 110-112 °C and 98% yield.

FTIR (KBr, cm^{-1}): 3443 (O-H), 3066 (aromatic C-H), 1620 (aromatic C=C), 1406 (N=N_{str}), 1070 (C-O)

UV/Vis λ_{max} (nm): 262 (π-π*), 399 (Inter-molecular charge transfer, IMCT) and 415 (n-π*)

^{1}H-NMR (DMSO-d_6) δ: 8.89 (s, 1H, H_g), 7.75 (d, 2H, H_e), 7.62 (d, 2H, H_d), 7.55 (m, 3H, H_c), 6.42 (d, 2H, H_b), 2.50 (s, 3H, H_a)

^{13}C-NMR (DMSO-d_6) δ: 145 (s), 130 (d), 129 (m), 127 (s)

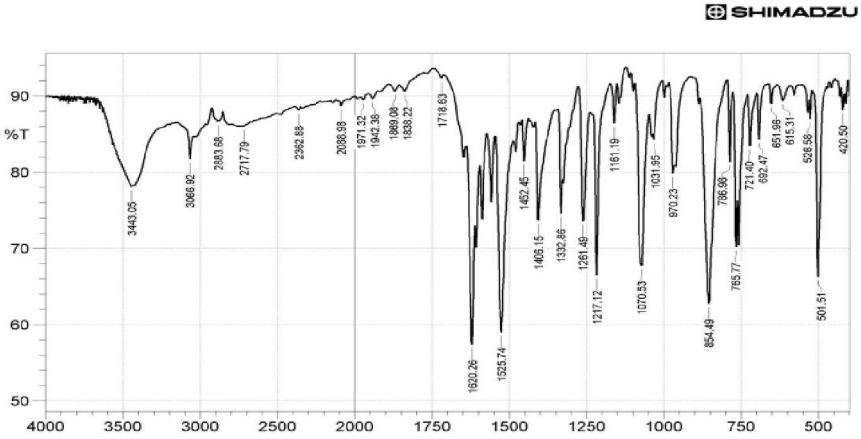

Figure 2: The FTIR spectrum of NAD

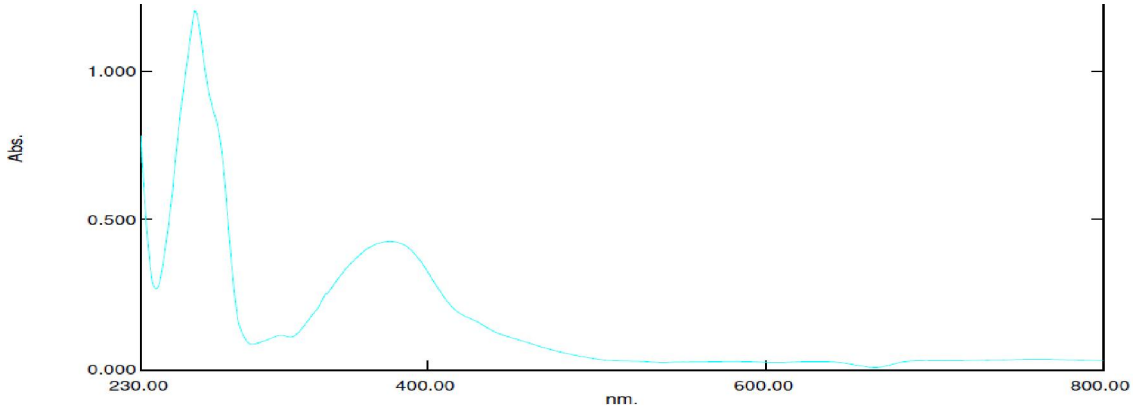

Fig. 3: The UV spectrum of NAD

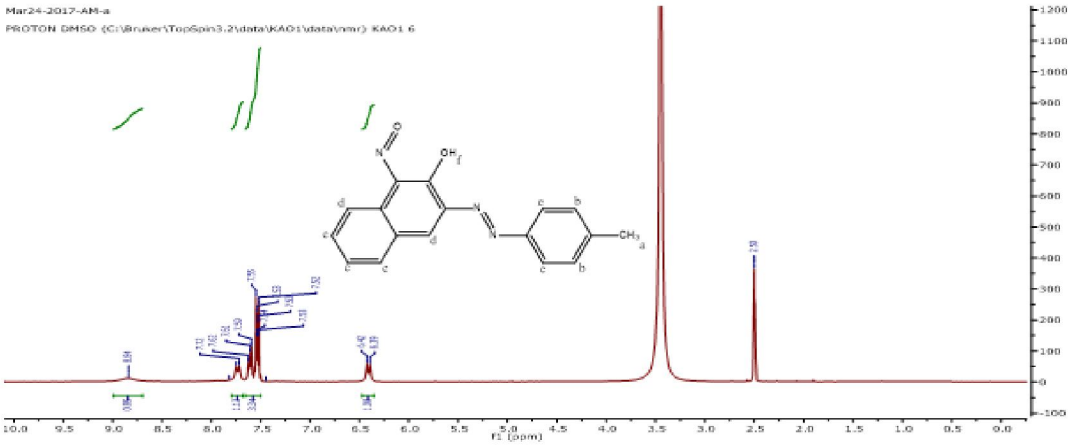

Figure 4: [1]HNMR spectrum of NAD

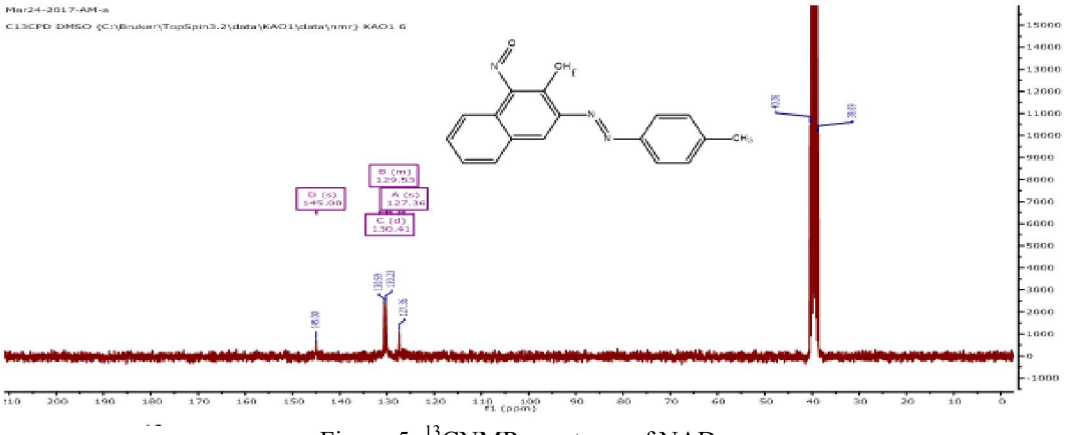

Figure 5: [13]CNMR spectrum of NAD

2.3 Preparation of solution

0.5 M HCl was prepared using hydrochloric acid of standard grade and distilled water which serve as the corrodent. The inhibitor (NAD) was added to this test solution in a dosage of 10 – 50 ppm. Steel coupons for the gravimetric experiment were introduced into beakers containing this tested solution and the tests were performed in thermostated water bath at each test temperature (25, 35, 45, 55 and 65^{o}C) for 6 hrs.

2.4 Weight loss experiment

The pre-treated Mild steel coupons weighed with the aid of analytical balance (0.0001 sensitivity) were immersed in 100 ml 0.5 M HCl test solution loaded with different concentrations of the inhibitor (10 – 50 ppm) in an open beaker for 6 hours at varying temperature (298 – 338 K at 10 K interval) using thermostated water bath. Samples were withdrawn from the test solution after 6 hrs, brushed with brittle brush, washed with distilled water, rinsed in acetone and dried in oven for 15 mins at 40 ^{o}C before reweighing (Geethamani and Kasthuri, 2015). Each of this experiment was performed in triplicate for accurate results and the mean of the final weight was used in the calculation. From the weight loss results, the corrosion rate, C_R, degree of surface coverage, θ and the percentage inhibition efficiency, IE % were determined using Equations 1, 2 and 3 respectively.

$$C_R = \frac{W_o - W_1}{At} \quad (1)$$

$$\theta = 1 - \frac{C_R{}^i}{C_R{}^o} \quad (2)$$

$$\%IE = \theta x 100 \quad (3)$$

Where W_o and W_1 are the weight loss (g) of mild steel in the absence and presence of the inhibitor respectively. A is the area of the mild steel (cm^2), t is the immersion time (hrs). $C_R{}^i$ and $C_R{}^o$ are the corrosion rates (g cm^{-2} hr^{-1}) in the presence and absence of the inhibitor respectively.

2.5 Potentiodynamic polarization experiments

Electrochemical experiments were conducted in a three-electrode cell using corrosion Lab and Versa stat 4 software under standard condition. A platinum sheet was used as the counter electrode (CE), saturated calomel electrode (SCE) as the reference electrode, while the mild steel machined into rectangular specimens with an exposed area of 1 cm^2 as the working electrode (WE). All potentials were measured against the SCE (0.2412 V with respect to the normal hydrogen electrode). Measurements were carried out in naturally aerated and unstirred solutions at 298 K using a thermostated water bath. The open current potential (OCP) was established by immersing the working electrode in the test solution for 10 mins while the potentiodynamic polarization studies were carried out by sweeping the applied potential from -250 mV to +250 mV at OCP with a scan rate of 1mVs^{-1} while the current, *I*, is recorded.

2.6 Computational studies

Quantum chemical calculations were performed on the most stable conformer of NAD after a conformation search has been carried out using the molecular mechanic force field (MMFF) method. The geometry of the molecule was optimized using the DFT with B3LYP correlation and a high basis set, 6-31G* using computational chemistry software. The energies of the frontier molecular orbitals, FMOs (HOMO and LUMO) were obtained, it affords us to understand the sites that are prone to nucleophilic and electrophilic attack and also used to determine the energy band gap, E_g (E_{LUMO} - E_{HOMO}) (Oyeneyin, 2017; Kara *et al.,* 2012; Anawe *et al.,* 2015). Other properties like the global reactivity descriptors like the chemical hardness (η), softness (δ), electronegativity (χ) and global electrophilicity index (ω) were calculated from the FMOs. The dipole moment (μ) and the fraction of electron transferred (ΔN) were also calculated, all in gas phase.

3. Results and Discussion

3.1 Gravimetric analysis

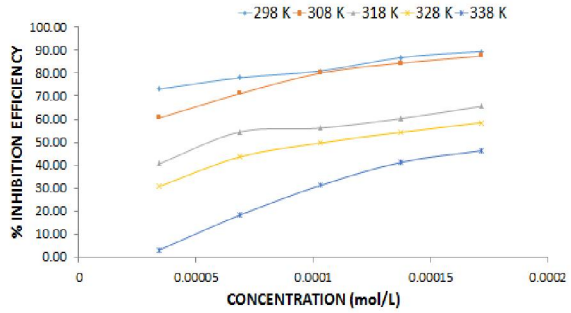

Figure 6: Variation of inhibition efficiency with concentration of NAD

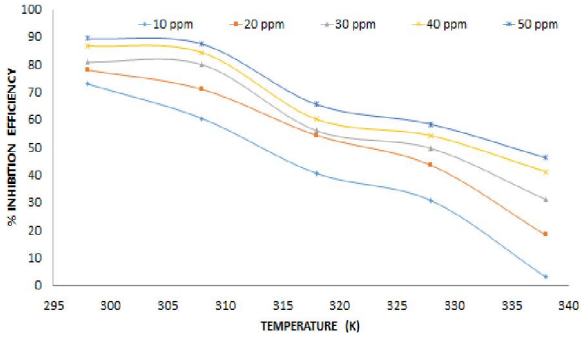

Figure 7: Variation of inhibition efficiency of NAD with temperature

In this work, gravimetric analysis was carried out at 298, 308, 318, 328 and 338 K using 0.5 M HCl as the corrodent. The results obtained showed that at different concentrations of NAD (0.00005, 0.0001, 0.00015 and 0.0002) mol/L, the % inhibition efficiency increases as the concentration of the inhibitor increases at a fixed temperature but reduces as the temperature is increased i.e the corrosion rate

reduces with an increase in concentration at a fixed temperature and increases with an increase in temperature (Figures 6 and 7). This is in line with what researchers observed in their work (Arukalam *et al.,* 2014; Ameh *et al.,* 2015; Aloysius *et al.,* 2017).

3.2 Adsorption considerations

The adsorption of an inhibitor on metal surface is in form of a substitution reaction, with the inhibitor substituting the water molecules adsorbed on the metal surface and in order to describe this reaction, adsorption isotherms are usually employed. The Langmuir adsorption isotherm (Equation 4) was employed in this study to explain the adsorption of NAD on the mild steel (Li *et al.,* 2010; Deng and Li, 2012).

$$C/\theta = \left[1/K_{ads}\right] + C \qquad 4$$

Where C is the concentration of inhibitor, K_{ads} the equilibrium adsorption constant and Θ the extent of surface coverage. The plot of C/Θ against C at different temperatures (298 – 338 K) gave the parameters listed in Table 3.1 while Figure 8 showed these plots. Both linear correlation coefficients (R^2) and slope values are closer to 1, suggesting that the adsorption obeys Langmuir adsorption isotherm. The little deviation from unity observed in the slope may be traced to the repulsion force in the adsorption layer (Mu et al., 2006).

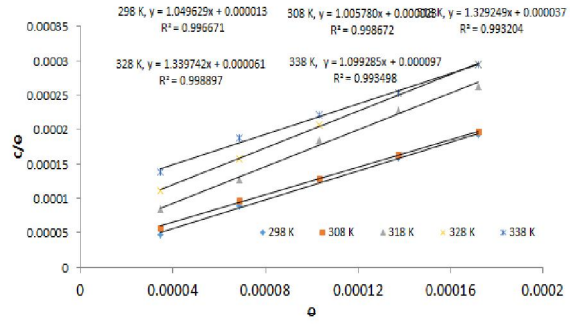

Figure 8: Langmuir adsorption isotherm plots for NAD adsorption

The decrease in the adsorptive equilibrium constant (K_{ads}) values with temperature gave an indication that at relatively lower temperatures, strong adsorption of NAD molecules onto the mild steel surface occurred. On the other hand, already adsorbed molecules of NAD got desorbed from the mild steel surface as experimental temperature increases (Deng and Li, 2012). To further explain the adsorption process, thermodynamic parameters were calculated. A relation (equation 5) was used to calculate the standard Gibb's free energies of adsorption (ΔG^o_{ads}) from the various values of adsorptive equilibrium constant at specific temperature (K_{ads}) (Stoyanova *et al.,* 1977).

$$K_{ads} = \frac{1}{55} e^{-\frac{\Delta G^0_{ads}}{RT}} \qquad 5$$

Where R is universal gas constant, ΔG_{ads} is the free energy of adsorption and 55.5 is the molar concentration of water in the solution known as the isocratic contribution. A plot of ΔG^o_{ads} against temperature using Equation 6 gave the enthalpy, ΔH^o and entropy ΔS^o of adsorption as intercept and slope respectively (Fiori-Bimbi *et al.,* 2015).

$$\Delta G^o_{ads} = \Delta H^o - T\Delta S^o \qquad 6$$

From the plot (Figure 9), -41.861 kJ mol^{-1} and -0.0136 kJ $mol^{-1}K^{-1}$ were obtained for ΔH^o_{ads} and ΔS^o_{ads}, respectively (Table 3.3).

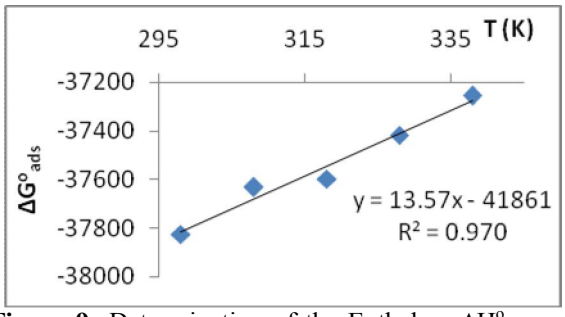

Figure 9: Determination of the Enthalpy, ΔH^o_{ads} and Entropy, ΔS^o_{ads}, of Adsorption of NAD on the Mild Steel Surface in 0.5 M HCL

Table 3.3: Values from Langmuir adsorption isotherm and thermodynamics study

Compd	Temp. (K)	R^2	Slope	1/K (mol/l)	K (l/mol)	ΔG (kJ/mol)	ΔS (kJ/mol K)	ΔH (kJ/mol)
NAD	298	0.996671	1.049629	0.000013	76923.08	-37.8249	-0.01357	-41.861
	308	0.998672	1.00578	0.000023	43478.26	-37.6332		
	318	0.993204	1.329249	0.000037	27027.03	-37.5982		
	328	0.998897	1.339742	0.000061	16393.44	-37.4171		
	338	0.993498	1.099285	0.000097	10309.28	-37.2544		

ΔG^o_{ads} were obtained as negative owing to spontaneity of adsorption. In general, value of ΔG^o_{ads} around -20 $kJmol^{-1}$ indicates physical adsorption and value of ΔG^o_{ads} of -40 kJ/mol and above is an indication of chemisorption (El-lateef, 2015). ΔG^o_{ads} obtained in this study were around -37 kJ/mol which

gave a hint of complex adsorption mechanism. The negative value of ΔS^{o}_{ads} showed the decrease in the degree of translational freedom of the molecules as it is being adsorbed on the mild steel surface. Negative value of ΔH^{o}_{ads} obtained indicated the exothermic nature of the adsorption process (Fiori-Bimbi et al., 2015). To differentiate physisorption from chemisorptions in an exothermic adsorption process, ΔH^{o}_{ads} around -40 kJmol^{-1} is an indication of physisorption while, ΔH^{o}_{ads} tending to -100 kJmol^{-1} indicates chemical adsorption of the inhibitor molecules. -41.801 kJ/mol obtained for ΔH^{o}_{ads} can be assigned to physical adsorption of NAD molecules on the mild steel surface.

3.3 Kinetic Studies and Activation Parameters

The adsorption behaviour of NAD was further explained using the kinetic model. The apparent activation energies, E_a, for the corrosion process and the pre-exponential factors, A, were determined using the plot of $\ln C_R$ against 1/T (Figure 10) as given by the Arrhenius equation 7 (Tu *et al.,* 2012). Values obtained are given in Table 3.4.

$$C_R = Ae^{-\frac{E_a}{RT}} \quad 7a$$

$$InC_R = InA - \frac{Ea}{RT} \quad 7b$$

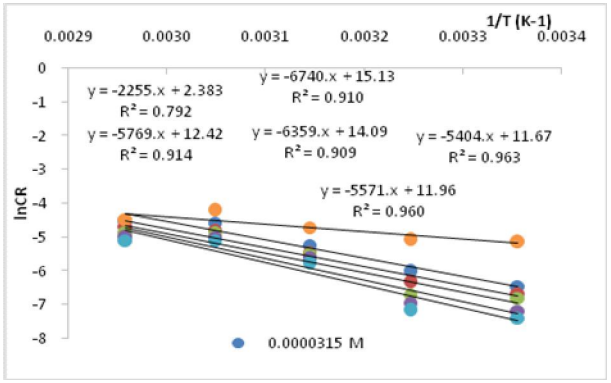

Figure 10: Apparent Activation Energy Determination for the Corrosion Process in 0.5 M HCl in the absence and presence of NAD

Table 3.4: Activation energy, E_a and pre-exponential factor A for the corrosion process in 0.5 M HCl.

Compd	Concentration (ppm)	Slope	E_a (J/mol)	lnA	A
NAD	BLANK	-2255.8	18754.72	2.3831	10.83845
	0.0000344	-5404.8	44935.51	11.673	117359.8
	0.0000687	-5571.8	46323.95	11.968	157629.1
	0.0001031	-5769.2	47965.13	12.423	248450.8
	0.0001375	-6359.8	52875.38	14.09	1315859
	0.0001718	-6740.5	56040.52	15.137	3749001

Values of apparent activation energies were observed to increase in the presence of NAD than that of pure acidic medium and increase as the concentration of NAD increases indicating the adsorption of the inhibitor molecules on most active adsorption sites with lowest energy while the corrosion takes place mainly on the active sites having higher energy and these adsorption increases as the concentration of NAD increases (Tu *et al.,* 2012). Higher energies are required for the corrosion reaction as the concentration of NAD increases in the inhibited solution. The higher values of E_a also indicate the physiadsorption that occurred in the first stage (Chen *et al.,* 2011; Tu *et al.,* 2012). The pre-exponential factor, A, in the Arrhenius equation is related to the number of active centers (Tu *et al.,* 2012). The larger values of A in the presence of NAD compared to that of the unhibited solution (Table 3.4) implied that most of the active sites are blocked by the adsorption of the inhibitor (Tu *et al.,* 2012).

Using the transition state Equation 8, values of enthalpy, ΔH^* and entropy, ΔS^* of activation were calculated using the slope and intercepts of the plots of $\ln (C_R/T)$ against 1/T (Figure 11) and these are given in Table 3.5.

$$C_R = \left(\frac{RT}{Nh}\right)\exp\left(\frac{\Delta S^*}{R}\right)\exp\left(\frac{-\Delta H^*}{RT}\right) \quad 8$$

Where h is the Planks' constant, N the Avogadro's number, T the absolute temperature and R the universal gas constant.

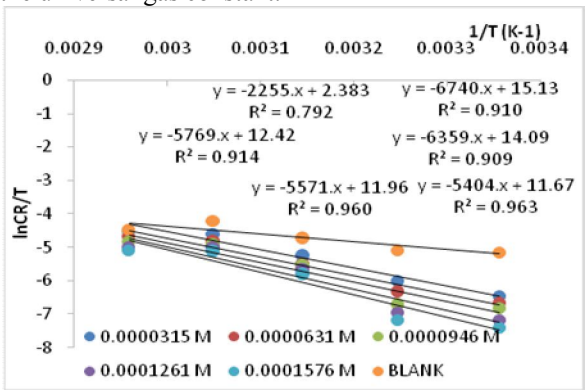

Figure 11: Transition state determination of enthalpy and entropy of activation in 0.5 M HCl in the absence and presence of NAD

Table 3.5: Values for the corrosion activation parameters of mild steel in 0.5 M HCl in the absence and presence of different concentration of NAD

Compd	Conc. (m)	Slope	Intercept	Enthalpy (J/mol)	Entropy ($Jmol^{-1}k^{-1}$)
NAD	BLANK	-3337	-0.344	27743.818	-200.4000
	0.0000344	-5472	5.661	45494.208	-150.4744
	0.0000687	-5407	5.400	44953.798	-152.6444
	0.0001031	-5313	5.048	44172.282	-155.5709
	0.0001375	-5170	4.539	42983.380	-159.8027
	0.0001718	-5034	4.055	41852.676	-163.8267

Analysis of data in Table 3.5 revealed an increase in ΔH* and ΔS* values in the presence of NAD an indication of the increase in energy barrier of corrosion process in the presence of NAD (Tu *et al.,* 2012) which agreed with the values of activation energy, E_a, presented in Table 3.4. Positive values of enthalpies of activation ΔH* in the absence and presence of NAD suggested an endothermic nature of the mild steel dissolution (Obot and Obi-Egbedi, 2008; Szauer and Brandt, 1981; Dahmani *et al.,* 2010; Peme *et al.,* 2015). Negative values obtained for ΔS* in the absence and presence of NAD suggested the formation of the activated complex in the rate determining step to be associative rather than been dissociative and hence, there was decrease in disorderliness as the reaction moves from the reactants to the activated complex (Peme *et al.,* 2015; Saliyan and Adhikari, 2008).

3.4 Potentiodynamic polarization

The polarization curves of the mild steel in 0.5 M HCl solution in the absence and presence of different concentrations of NAD are given by Figure 12. Other parameters such as the corrosion potential (E_{corr}), corrosion current density (I_{corr}), anodic Tafel slope (β_a), cathodic Tafel slope (β_c) and percentage inhibition efficiency (% IE) are summarized in Table 3.6. Equation 9 helped to give the inhibition efficiency calculated from the values of corrosion current density extrapolated from the tafel curves (Chen *et al.,* 2011).

$$\%IE = \frac{I^0_{corr} - I_{corr}}{I^0_{corr}} x100 \qquad 9$$

Where, I^0_{corr} and I_{corr} are the corrosion densities in the absence and presence of the inhibitor respectively.

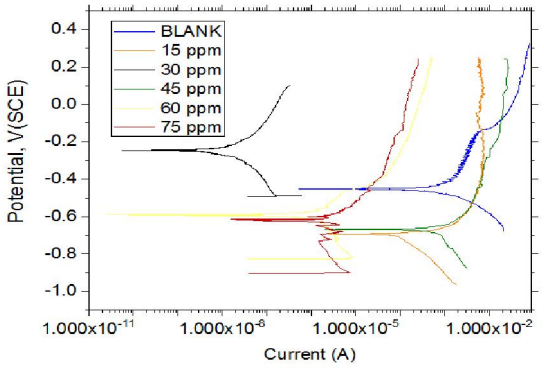

Figure 12: Potentiodynamic polarisation curve for mild steel in 0.5 M HCl solution in the absence and presence of NAD**.**

Table 3.6: Polarization parameters and inhibition efficiencies for mild steel in 0.5 M HCl solution in the absence and presence of different concentrations of NAD at 298 K

Compd	Conc (g)	- β_c (mV)	β_a (mVdec-1)	C_R mpy	-E_{corr} (mV)	I_{corr} (mA)	% IE
NAD	Blank	111.71	292.71	461.40	451.4	1.009000	-
	0.015	248.49	55.83	76.15	703.2	0.166000	83.55
	0.030	148.03	148.03	0.0059	248.1	0.000012	99.99
	0.045	269.854	221.63	397.36	703.1	0.869803	13.80
	0.060	146.87	146.87	0.4835	594.3	0.001058	99.90
	0.075	270.91	270.91	2.253	618.4	0.004931	99.51

Generally, organic inhibitors can be classified as cathodic, anodic or mixed-type inhibitor depending on whether there is decrease in the corrosion current densities at the cathodic or anodic or both sides, respectively, of the Tafel curves on addition of the inhibitor (Hu *et al.,* 2013; Chen *et al.,* 2013). It was observed from Figure 3.6 that both the cathodic and the anodic corrosion current densities decreased

considerably most especially in the presence of 30 ppm NAD indicating that NAD is a mixed type inhibitor. This suggested that NAD has retarding effect on both cathodic and anodic half reactions. Analysis of data in Table 3.6 equally revealed changes in the values of β_a and β_c in the presence of NAD indicating the influence of the inhibitor on the anodic and cathodic reactions (Al-Amiery *et al.,* 2014). The displacement of E_{corr} to the more negative values in the presence of NAD suggested the retarding effect of the inhibitor on both sides of the tafel curve. Hence, the corrosion reaction of the mild steel is inhibited. An increase in the inhibition efficiency of NAD in the inhibited solution as compared to the uninhibited solution was also observed suggesting the adsorption of NAD on most of the active sites causing considerable decrease in the corrosion current of the mild steel.

3.5 Quantum Chemical calculations

The results obtained from the quantum chemical calculations were given in Table 3.7. The optimized structure, Highest Occupied Molecular Orbital (HOMO) and the Lowest Unoccupied Molecular Orbital (LUMO) of NAD are given by Figure 13. The energy band gap is 3.12 eV; indicative that there is an inherent electron donating ability and that there is an interaction between the inhibitor and the metal surface with high HOMO energy of -6.09 eV, indicative that the inhibitor has excellent donating ability and a low LUMO energy of -2.97 eV, indicative that the inhibitor can accept electrons from metal's *d* orbitals. The chemical hardness, a direct consequence of the energy band gap was calculated using Equation 10 Its value is 1.56 eV (Oyeneyin, 2017; Kara *et al.,* 2012; Anawe *et al.,* 2015);

$$\eta = \frac{E_g}{2} \qquad 10$$

Softness is the inverse of hardness and it determines the ability of a molecule to react. Soft molecules are more reactive than hard ones because of the ease with which they could offer electrons to an acceptor (Li *et al.,* 2015; Aloysius *et al.,* 2017). It is calculated according to Equation 11 (Oyeneyin, 2017; Kara *et al.,* 2012; Anawe *et al.,* 2015) and of a value of 0.64 eV^{-1}. The hard and soft acids and bases principle (HSAB) explains that soft acids tend to react with soft bases and hard acids with hard bases. A bulk metal, whose chemical hardness is assumed to be zero very soft, a soft acid, therefore, they tend to react with soft bases (in this case, the inhibitor). This means that the inhibitor must have a high softness value; this enhances high adsorption and hence high corrosion inhibition efficiency (Li *et al.,* 2015, Aloysius *et al.,* 2017).

$$\delta = \frac{1}{\eta} \qquad 11$$

Other global reactivity descriptors calculated are the electronegativity in Equation 12 (Oyeneyin, 2017; Kara *et al.,* 2012; Anawe *et al.,* 2015). NAD has 4.53 eV as its electronegativity, a value lower than that of iron as expected.

$$\chi = \frac{I+A}{2} \qquad 12$$

Where; I = $-E_{HOMO}$ and A = $-E_{LUMO}$ and the global electrophilicity index in Equation 13

$$\omega = \frac{\chi^2}{E_g} \qquad 13$$

A good inhibitor is characterized by donation of electrons from its HOMO orbitals to the metal's *d* orbitals and also through the acceptance of electrons from the metal's *d* orbitals to its orbitals.

Fraction of electron transferred was calculated using Equation 14 (Oyeneyin, 2017; Kara *et al.,* 2012).

$$\Delta N = \frac{\chi_{Fe} - \chi_{inh}}{2\,(\eta_{Fe} + \eta_{inh})} \qquad 14$$

Where, χ_{Fe} and χ_{Inh} are the electronegativities of iron (representing bulk metal) and the inhibitor molecule respectively. η_{Fe} and η_{Inh} are the absolute hardness of iron and the inhibitor molecule respectively. χ_{Fe} has a theoretical value of 7 eV while that of η_{Fe} is 0 eV (Oyeneyin, 2017; Anawe *et al.,* 2015) As the inhibitor is brought in contact with the bulk metal, electrons flow from the lower χ_{Inh} to the higher χ_{Fe}. ΔN represents the inhibition effect resulting from electron donations and inhibition efficiency can be seen as effective if $\Delta N < 3.6$ (Li *et al.,* 2015; Lukovits *et al.,* 2001). ΔN for NAD is 0.79, an indication that it has the ability to donate electrons. This has been earlier confirmed by the low hardness and high softness values.

Also, the dipole moment is an important parameter to ascertain if electrons are distributed in the molecular structure and if there is a strong dipole-dipole interaction between NAD and the metal surface. NAD has a dipole moment of 4.49 Debye, an indication that the inhibition absorption is enhanced through electronic force (Zhang *et al.,* 2012)

Table 3.7: Quantum chemical parameters for NAD dye

Properties	E_{HOMO} (eV)	E_{LUMO} (eV)	E_g (eV)	η (eV)	δ(eV^{-1})	χ(eV)	ω(eV)	μ(D)	ΔN
NAD	-6.09	-2.97	3.12	1.56	0.64	4.53	6.58	4.49	0.79

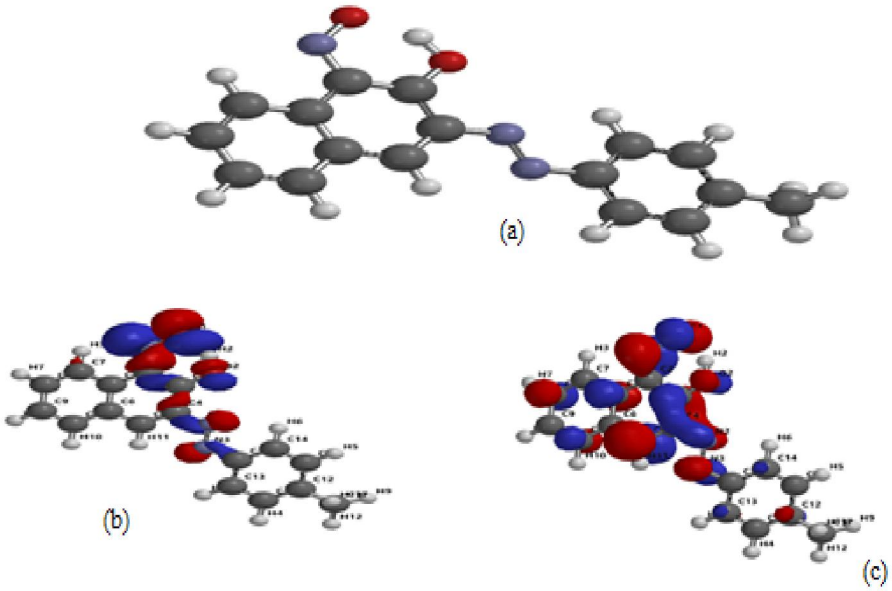

Figure 13: a. Optimized Structure, b. Highest Occupied Molecular Orbital (HOMO) and c. the Lowest Unoccupied Molecular Orbital (LUMO) of NAD.

4. Conclusions

The study synthesised and characterised (E)-3-(2-P-Tolyldiazenyl)-1-Nitrosonaphthalen-2-ol with its inhibitory performance evaluated using gravimetric and electrochemical methods. It also described NAD as a good inhibitor for mild steel in acidic environment with Inhibition efficiency increasing with increase in concentration and decreasing with increase in temperature. Electrochemical measurement using potentiodynamic polarization revealed a mixed-type organic inhibitor. Considerable inhibitory efficiencies were obtained using potentiodynamic polarization in the presence of NAD, indicating good agreement with that by weight loss. The adsorption of NAD on mild steel obeys Langmuir adsorption isotherm and is an exothermal and entropy decreasing process while the adsorption mechanism follows physical adsorption. The values of activation parameters (E_a, ΔH* and ΔS*) increased in the presence of NAD. Hence, conclusion could be made that the adsorbed NAD molecules blocked the active sites of lower energy and inhibited the mild steel dissolution. The quantum chemical study showed that NAD possessed a strong electron donating and accepting properties which enhanced its strong adsorption on the metal surface.

Conflict of interest: None

Acknowledgements

All Authors in this work hereby expressed their profound gratitude to Tertiary Education Trust Fund (TET Fund) for supporting this work.

Corresponding Author
Dr. O. F. Akinyele
Department of Chemistry,
Obafemi Awolowo University, Ile-Ife, Nigeria
Telephone: 08023410301
E-mail: ofakinyele@oauife.edu.ng

References

1. Abiola OK, Otaigbe JOE. The effects of Phyllanthusamarus extract on corrosion and kinetics of corrosion processes of aluminium in alkaline solution. Corros Sci. 2009; 51: 2790-3.
2. Abiola OK, Otaigbe JOE. Adsorption behavior of 1-phenyl-3-methylpyrazol-5-one on mild steel from HCl solution. Int J Electrochem Sci. 2008; 3: 191-8.
3. Obot IO, Obi-Egbedi NO. Inhibitive properties, thermodynamic and quantum chemical studies of

alloxazine on mild steel corrosion in H_2SO_4. Corrosion Science 2011;53:263-75.
4. Arukalam IO, Madufor IC, Ogbobe O, Oguzie E. Experimental and Theoretical Studies of Hydroxyethyl Cellulose as Inhibitor for Acid Corrosion Inhibition of Mild Steel and Aluminium. The Open Corrosion Journal. 2014; 6: 1-10.
5. Solmaz R. Investigation of corrosion inhibition mechanism and stability of Vitamin B1 on mild steel in 0.5 M HCl solution. Corros Sci. 2014; 81: 75-84.
6. Ameh PO, Koha PU, Eddy NO. Experimental and Quantum Chemical Studies on the Corrosion Inhibition Potential of Phthalic Acid for Mild Steel in 0.1 M H_2SO_4. Chemical Science Journal. 2015; 6; 3: 1-8.
7. Oguzie EE, Enenebeaku CK, Akalezi CO, Okoro SC, Ayuk AA. Adsorption and corrosion-inhibiting effects of Dacryodis edulis extract on low-carbon-steel corrosion in acidic media. J Colloid interface Sci. 2010; 349: 283-292.
8. Naguib A. M, Mahross MH, Khalil H. F. Y, Mahran BNA, Yehia MM, El-Sabbah MMB. Azo Dye Compounds as Corrosion Inhibitors for Dissolution of Mild Steel in Hydrochloric Acid Solution. Portugaliae Electrochimica Acta. 2013; 31(2):119-139.
9. Mabrouk EM, Eid S, Attia MM. Corrosion inhibition of carbon steel in acidic medium using azo chromotropic acid dye compound. Journal of Basic and Environmental Sciences 2017; 4: 351-355.
10. Fouda AS, El-Azaly AH, Awad RS, Ahmed AM. New Benzonitrile Azo Dyes as Corrosion Inhibitors for Carbon Steel in Hydrochloric Acid Solutions. International Journal of Electrochemical Science 2014; 9: 1117-1131.
11. Oyeneyin OE. Structural and Solvent Dependence of the Electronic Properties and Corrosion Inhibitive Potentials of 1,3,4-thidiazole and Its Substituted Derivatives- A Theoretical Investigation. Physical Science International Journal 2017; 16(2): 1-8.
12. Kara YS, Seda GS, Esme A. Theoretical Study on the Relationship between the Molecular Structure and Corrosion Inhibition Efficiency of Long Alkyl Side Chain Acetamide and Isoxazolidine Derivatives. Protection of Metals and Physical Chemistry of Surfaces. 2012; 48(6): 710-721.
13. Elmsellem H, Aouniti A, Khoutoul M, Chetouani A, Hammouti B, Banchat N, Touzani R, Elazzouzi M. Theoretical approach to the corrosion inhibition efficiency of some pyrimidine derivatives using DFT method of mild steel in HCl solution. Journal of Chemical and Pharmaceutical Research. 2014; 6(4): 1216-1224.
14. Anawe PAL, Obi CU, Mehdi SS, Ogunniran KO, Ita BI, Ehi-Oromosele CO. Experimental and Theoretical Studies of (E)-N'-1-(4-propylbenzylbenzylidene) nicotinohydrazide as Corrosion Inhibitor of Mild Steel in HCl. 2015; 51(3):458-466.
15. Li X, Xie X, Deng S, Du G. Inhibition effect of two mercaptopyrimidine derivatives on cold rolled steel in HCl solution. Corrosion Science 2015;92:136-147.
16. Aloysius A, Ramanathan R, Christy A, Baskaran S, Antony N. Experimental and Theoretical Studies of vitamins- Thiamine hydrochloride or biotin in corrosion of mild steel in aqeous chloride environment. Egyptian Journal of Petroleum 2017 (in press).
17. Lukovits I, Kalman E, Zucchi F. Corrosion Inhibitors: Correlation between the electronic structures and efficiency. Corrosion Science 2001; 57: 3.
18. Zhang F, Tang Y, Cao Z, Jing W, Wu Z, Chen Y. Performance and theoretical study on corrosion inhibition of 2-(4-pyridyl)-benzimi- dazole for mild steel in hydrochloric acid. Corros Sci. 2012; 61:1-9.
19. Geethamani P, Kasthuri PK. Adsorption and corrosion inhibition of mild steel in acidic media by expired pharmaceutical drug. Cogent Chemistry 2015; 1(1): 1091558.
20. Botros RUS. Patent No. 4,051,119. Washington 1977, DC: U.S. Patent and Trademark Office.
21. Ahmadi RA, Amani S. Synthesis, spectroscopy, thermal analysis, magnetic properties and biological activity studies of Cu (II) and Co (II) complexes with Schiff base dye ligands. Molecules 2012;17(6):6434-6448.
22. Li XH, Deng SD, Fu H. Inhibition by Jasminum nudiflorum Lindl. leaves extract of the corrosion of cold rolled steel in hydrochloric acid solution, Journal of Applied Electrochemical 2010; 40:1641–1649.
23. Deng S, Li, X. Inhibition by Jasmium nudiflorum Lindl. Leaves extract of the corrosion of aluminium in HCl solution. Corrosion Science 2012;64:253-262.
24. Mu GN, Li XH, Qu Q, Zhou J. Molybdate and tungstate as corrosion inhibitors for cold rolling steel in hydrochloric acid solution, Corrosion Science 2006; 48: 445–459
25. Stoyanova AE, Sokolova EI, Raicheva SN. The inhibition of mild steel corrosion in 1 M HCL in the presence of linear and cyclic thiocarbamides—Effect of concentration and

temperature of the corrosion medium on their protective action, Corrosion Science 1977; 39:1595–1604.
26. Fiori-Bimbi MV, Alvarez PE, Vaca H, Gervasi CA. Corrosion inhibition of mild steel in HCL solution by pectin. Corrosion Science 2015;92:192-199.
27. El-Lateef HMA. Experimental and computational investigation on the corrosion inhibition characteristics of mild steel by some novel synthesized imines in hydrochloric acid solutions. Corrosion Science 2015; 92:104-117.
28. Tu S, Jiang X, Zhou L, Wang H, Jiang X. Synthesis of N-alkyl-4-(4-hydroxybut-2-ynyl) pyridinium bromides and their corrosion inhibition activities on X70 steel in 5M HCl. Corrosion Science 2012;65:13-25.
29. Chen W, Luo HQ, Li NB. Inhibition effects of 2, 5-dimercapto-1, 3, 4-thiadiazole on the corrosion of mild steel in sulphuric acid solution. Corrosion Science 2011;53(10):3356-3365.
30. Obot IB, Obi-Egbedi NO. Fluconazole as an inhibitor for aluminium corrosion in 0.1 M HCl. Colloids and Surfaces a: Physicochemical and Engineering Aspects 2008; 330(2):207-212.
31. Szauer T, Brandt A. Adsorption of oleates of various amines on iron in acidic solution. Electrochimica Acta 1981; 26(9):1253-1256.
32. Dahmani M, Et-Touhami A, Al-Deyab SS, Hammouti B, Bouyanzer A. Corrosion inhibition of C38 steel in 1M HCl: A comparative Study of Black Pepper Extract and its isolated piperine. International Journal of Electrochemical Science 2010; 5: 1060-1069.
33. Peme T, Olasunkanmi LO, Bahadur I, Adekunle AS, Kabanda MM, Ebenso EE. Adsorption and corrosion inhibition studies of some selected dyes as corrosion inhibitors for mild steel in acidic medium: gravimetric, electrochemical, quantum chemical studies and synergistic effect with iodide ions. Molecules 2015; 20(9): 16004-16029.
34. Saliyan R, Adhikari AV. Inhibition of corrosion of mild steel in acid media by N'-benzylidene-3-(quinolin-4-ylthio) propanohydrazide. Bulletin of Materials Science 2008;31(4).
35. Chen ZY, Li LJ, Zhang GA, Qiuand YB, Guo XP. Inhibition effect of propargylalcohol on the stress corrosion cracking of super 13Cr steel in a completion fluid, Corrosion Science 2013;69:205–210.
36. Hu JY, Zeng DZ, Zhang Z, Shi TH, Song GL, Guo XP. 2-Hydroxy-4-methoxy-acetophenone as an environment-friendly corrosion inhibitor for AZ91D magnesium alloy, Corrosion Science 2013; 74:35–43.
37. Al-Amiery AA, Kadhum AAH, Kadihum A, Mohamad AB, How, CK, Junaedi S. Inhibition of Mild Steel Corrosion in Sulfuric Acid Solution by New Schiff Base. Materials 2014;7:787 – 804.

11/19/2020